



Ion Channels

How to cite: Angew. Chem. Int. Ed. **2025**, e202519101 doi.org/10.1002/anie.202519101

Rhodopsin-Mimicking Reversible Photo-Switchable Chloride Channels Based on Azobenzene-Appended *Semiaza*-Bambusurils for Light-Controlled Ion Transport and Cancer Cell Apoptosis

Lei He, Yuanhong Ma, Yang Zhang, Canhong Zhu, Feihu Yang, Yuancheng Ji, Shengda Liu, Hui Li, Jiayun Xu, Pengfei Zhang, Tengfei Yan,* Ofer Reany,* and Junqiu Liu*

Abstract: The ability to control ion transport across membranes in living systems by stimulus-responsive natural channels, such as channelrhodopsins and their mimics, is a revolutionary tool for understanding biological processes. Herein, we demonstrate a new class of azo-functionalized bambusurils (azo-BUs) that act as efficient, photo-switchable anion channels capable of modulating chloride flux across lipid membranes and within cellular environments. The (E)-isomer exhibits pronounced chloride transport activity, which can be reversibly toggled via light-induced isomerization, enabling precise spatiotemporal control. Mechanistic studies reveal that the (E)-form induces apoptosis through mitochondrial membrane depolarization, reactive oxygen spieces (ROS) generation, and cytochrome c release, while also disrupting lysosomal acidification via H^+/Cl^- cotransport. This dual perturbation of cytosolic and lysosomal ion homeostasis underscores the compound's multifaceted cytotoxic mechanism. In contrast, the (Z)-isomer displayed minimal transport activity and negligible cytotoxicity, reinforcing its role as the inactive, photo-switchable OFF state in this system. The ability to control transport activity with light positions azo-BUs as promising candidates for the development of next-generation, stimuli-responsive anticancer agents. This work introduces a reversible photo-gated anion channel with therapeutic potential, offering a powerful platform for studying membrane transport and designing light-responsive biomedical tools.

Introduction

The passage of physiologically relevant substances across plasma membranes is a fundamental process essential for maintaining cellular function and internal homeostasis in biological systems.^[1,2] This process is often promoted by stimuli-responsive protein transporters, such as those sensitive to light,^[3] ligand binding,^[4] voltage,^[5] enzyme activation,^[6]

[*] L. He, Y. Ma, Y. Zhang, C. Zhu, Dr. F. Yang, Y. Ji, Dr. H. Li, J. Xu, Prof. P. Zhang, Dr. T. Yan, Prof. J. Liu

College of Material, Chemistry and Chemistry Engineering, Key Laboratory of Organosilicon Chemistry, and Material Technology, Ministry of Education, Zhejiang Key Laboratory of Organosilicon Material Technology, Hangzhou Normal University, Hangzhou 311121, China

E-mail: 20203011@hznu.edu.cn junqiuliu@hznu.edu.cn

L. He

School of Life and Environmental Sciences, Hangzhou Normal University, Hangzhou 311121, China

Dr. S. Liu

School of Chemistry and Environmental Engineering, University of Science and Technology, Changchun 130022, China

Prof. O. Reany

Natural Sciences, The Open University of Israel, 1, University Road, P.O. Box 808, Ra'anana 4353700, Israel E-mail: oferre@openu.ac.il

Additional supporting information can be found online in the Supporting Information section and mechanical forces.^[7] Naturally occurring rhodopsin, consisting of retinal and opsin, is a prominent photoreceptor protein involved in signal transduction, phototransduction, and retinal diseases.^[8] Specifically, bacteriorhodopsin^[9] and halorhodopsin^[10] are prototypical light-driven ion pumps that transport ions across cellular membranes via photo-induced conformational change. These transporter proteins undergo structural transformations in response to external stimuli, facilitating transmembrane transport and communication. This process reveals not only remarkable biological mechanisms but also serves as a profound source of inspiration for designing synthetic surrogates of stimulus-responsive transport systems.^[11–17]

Artificial light-driven ion transporters offer distinct advantages, including remote controllability, high spatiotemporal precision, and the absence of chemical by-products. In vitro studies of synthetic photo-responsive ion transporters serve as valuable tools for investigating the influence of light on ion transport behaviors and mechanisms in biomembranes, especially considering the fragility and instability of natural transporter proteins. However, replicating the reversible photo-regulating functionality of anion transport across membranes, akin to that observed in natural systems, remains a significant challenge due to the intricate design and demanding synthesis procedures. These challenges are reflected in the limited number of established systems that have been reported to date.^[18-23] Most current photo-responsive anion transport systems have been demonstrated only in liposome models, while photo-controlled ion transport in living cells is still in its infancy. Given that "smart", photo-controlled



properties are highly favorable for biomedical applications, the realization of photo-switchable anion transport in living cells is particularly attractive.

Fabricating artificial stimuli-responsive anion transporters is highly appealing but remains challenging due to the limited availability of suitable molecular building blocks. Among the various synthetic systems developed for anion transmembrane transport, including those based on hydrogen bonding, [24-29] halogen bonding, [30,31] chalcogen bonding, [32,33] and pnictogen bonding donors, [34] macrocyclic compounds have emerged as a beneficial scaffold in molecular host design.[35-41] A representative example of a cavitand is the bambus[6]uril (BU[6]), which exhibits a hydrophobic framework and twelve inward-facing anion-binding C-H bonds within the cavity, offering distinct advantages for transmembrane anion delivery.[42-44] For instance, Torrisi et al. reported that modifying the BU[6] structure with bile acid residues could lead to the formation of an unimolecular ion channel in membranes.^[45] In addition, hetero-BU[6] derivatives, such as semithio- and semiaza-BU[6]s, have emerged as promising candidates for anion transport activities. These structures offer enhanced membrane compatibility and structural versatility, enabling the easy incorporation of functional groups while avoiding the challenges of bottom-up synthesis.[46-48]

Channelrhodopsin regulates ion transmembrane transport through light-induced conformational isomerization, switching the channel between open and closed states. This mechanism is reminiscent of azobenzene, an effective molecular photoswitch that undergoes reversible photoisomerization, resulting in significant changes in molecular geometry and physicochemical properties. Several examples of photo-responsive conjugated azobenzene-macrocycles have demonstrated control over molecular transport processes using light as a stimulus. These conjugates undergo light-triggered conformational and amphiphilic changes, allowing for the regulation of cargo transport through azobenzene-type isomerization.^[49–52] Previous studies on structure-activity relationships have revealed that subtle modifications to semiaza-BU[6]s can lead to significant changes in their membrane-embedding ability and ion transport performance. [48] Drawing inspiration from the lightgated function of natural channelrhodopsin, we designed azobenzene-appended BU[6]s (azo-BUs) by grafting azobenzene units onto semiaza-BU[6] scaffolds (Scheme 1).

These molecules could function as light-regulated anion transporters, exhibiting photo-switchable transport activity in both liposome models and living cells through a single-molecular channel mechanism. Notably, this is a reversible ON/OFF photo-switchable anion channel.

Results and Discussion

Synthesis and Photoisomerization Behavior

The synthesis of *semithio*-BU[6] and *semiaza*-BU[6] derivatives has been previously described in studies on *hetero*-BUs, and follows a straightforward protocol.^[48,53]

Azobenzene-containing primary amines were synthesized via condensation of N-Boc-amino carboxylic acids with 4-aminoazobenzene, followed by Boc group removal (Schemes S2, 3a-f). Subsequent methylation of *semithio-BU*[6] yielded a reactive methyl thiouronium-based BU[6] triflate salt (Scheme S1, 5), which underwent nucleophilic substitution with **3a-f** to afford *semiaza-BU*[6] polyiminium salts (Schemes S3, 6a-f). Final neutralization using Amberlyst A26 resins produced the desired azo-BU[6]s (**7a-f**) in good yields. A 3D model of **7b** in its elongated structure was used to calculate the distances between the edges of the aromatic rings of the azobenzene groups on both sides of the portals. The calculated distance \approx 3.9 nm is sufficient to span across a typical bilayer membrane (Figure 1b). [47]

Azobenzene photoswitches are well known for undergoing conformational transformations and changes in polarity (dipole moment $\approx 3D$) upon illumination with a specific wavelength of light.^[54] The reversible photoisomerization behavior of the azo-BUs **7a–7f** was systematically investigated in an acetonitrile/DMSO mixture using UV–vis spectroscopy, and in deuterated DMSO via ¹H NMR spectroscopy. Across the series, the azo-BUs displayed absorption within a similar wavelength range (Figures 2a and S19–S24).

Upon brief exposure to 365 nm light, a decrease in absorption at approximately 375 nm was observed, accompanied by a modest increase at around $\lambda = 450$ nm, indicating isomerization from the (*E*)- to the (*Z*)-isomer. Subsequent irradiation with 450 nm light then reversed these spectral changes, restoring the (*E*)-isomer configuration. Notably, throughout multiple cycles of alternate 365/450 nm irradiations, this reversible process remained consistently robust, with no significant signs of decomposition of compound **7b** (Figures 2a and S25).

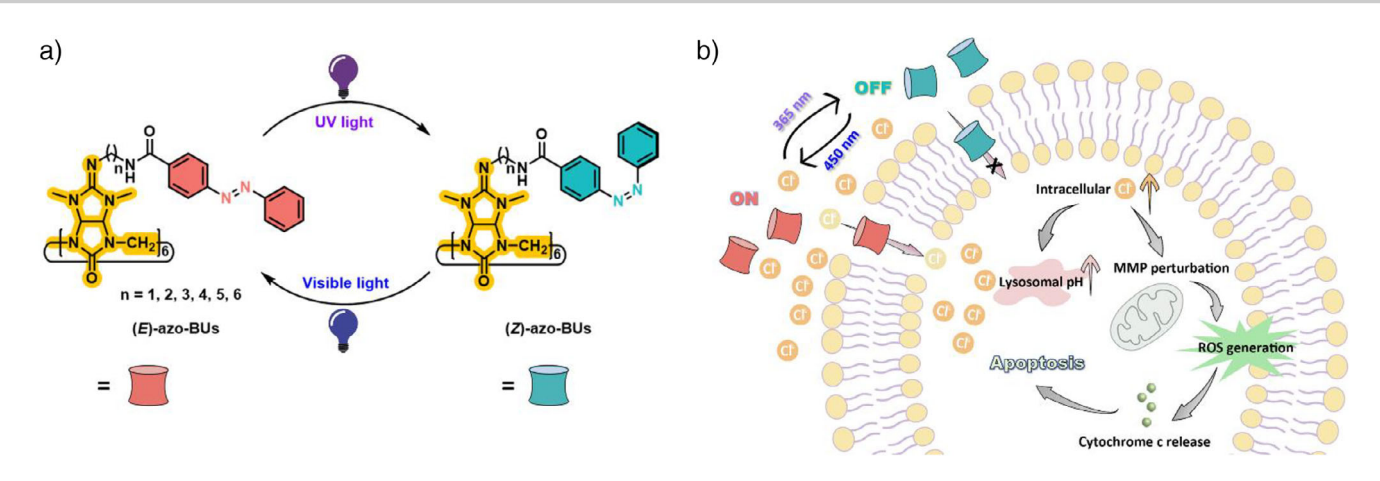
The photo-stationary state (PSS) ratios of azo-BUs were quantified by ¹H NMR spectroscopy in deuterated DMSO (Figures 2b and S27-S32). Upon 365 nm irradiation, new sets of signals appeared with upfield chemical shifts, consistent with E-to-Z isomerization and similar to spectral changes observed in other azobenzene photoswitches.^[55] As illustrated in Figures 2b and \$28, the integral ratio of the NH proton signals for compound 7b reached approximately 1:5 (E/Z) after 365 nm irradiation. Subsequent exposure to 450 nm light reversed the isomer distribution to an E/Z ratio of 4:1, confirming the reversible nature of the photoisomerization process. In agreement with the behavior of previous studies on azobenzene derivatives, (E)-7b also underwent partial thermal regeneration from the metastable (Z)-form in the dark, yielding a mixture of approximately 31% (E)- and 69% (Z)-isomers at ambient temperature (Figure \$33).

Anion Transport Activity

To test how well compounds **7a–7f** transport anions across membranes, we used large unilamellar vesicles (LUVs) composed of egg yolk lipids (EYPC). These vesicles were filled with 6-methoxy-N-(3-sulfopropyl)quinolinium (SPQ), a chloride-sensitive dye, and sodium nitrate, while the

15213773, 0, Downloaded from https://onlinelibrary.wiley.com/doi/10.1002/anie.202519101 by Hangzhou Normal University, Wiley Online Library on [10/11/2025]. See the Terms and Conditions (https://onlinelibrary.wiley.com/erms/

and-conditions) on Wiley Online Library for rules of use; OA articles are governed by the applicable Creative Commons License



Scheme 1. Reversible photo-switchable chloride channels for light-controlled ion transport and cancer cell apoptosis. **a)**. The structure of azobenzene-appended *semiaza*-bambusurils following irradiation with UVA and visible light, and **b)**. Schematic representation of the photo-controlled chloride transport across the phospholipidic membrane and cell apoptosis.

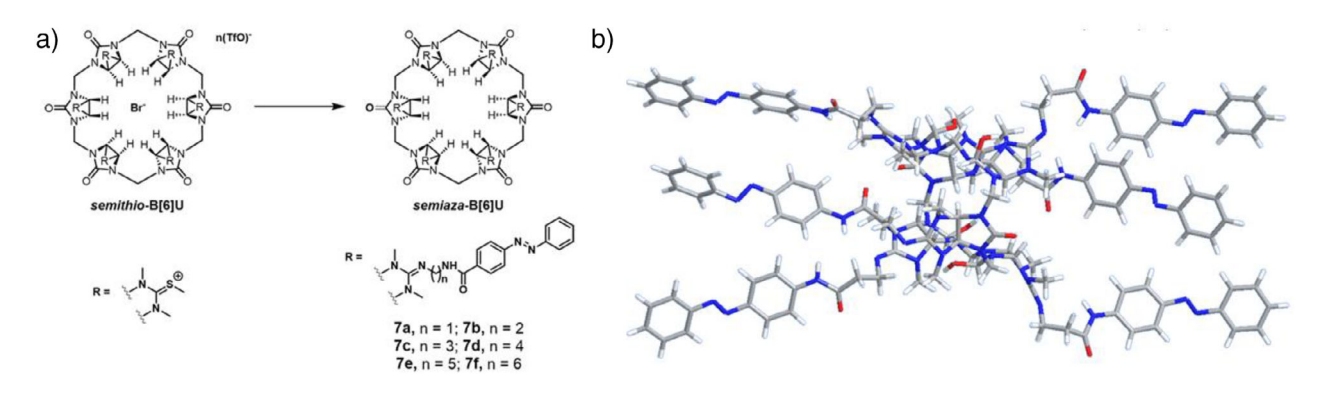


Figure 1. Synthesis of azo-BUs 7a-7f; a). The reactive methyl thiouronium-BU[6] in its triflate salt is transformed to semiaza-BU equipped with azobenzene linkers (see text); b). A 3D model of 7b demonstrating its elongated conformation at a calculated distance of 3.9 nm.

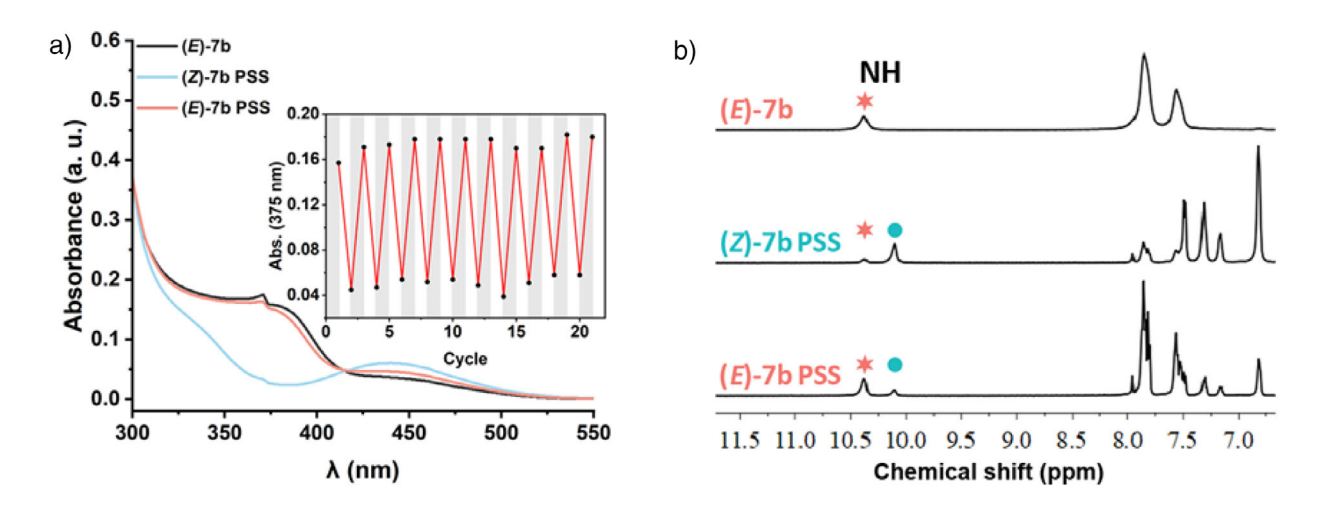


Figure 2. Photoisomerization and spectroscopic characterization of compound 7b: a). UV–vis spectra of (E)-7b (25 μM in acetonitrile) and its PSS after irradiation at 365 nm for 30 s, followed by irradiation at 450 nm for 10 s, demonstrating reversible photoisomerization. Inset: Cycling experiment showing consistent absorbance changes over multiple irradiation cycles, confirming the compound's photostability and reversibility. b). Partial 1 H NMR spectra (500 MHz, DMSO- d_6) of 7b before (top) and after irradiation with 365 nm (middle) for 30 min and then irradiation at 450 nm (bottom) for 10 min. The asterisks and filled circle indicate diagnostic peaks used to distinguish between the E and E isomers.

15213773, 0, Dov

vnloaded from https://onlinelibrary.wiley.com/doi/10.1002/anie.202519101 by Hangzhou Normal University, Wiley Online Library on [10/11/2025]. See the Terms and Conditions (https://onlinelibrary.wiley.com/

and-conditions) on Wiley Online Library for rules of use; OA articles are governed by the applicable Creative Commons

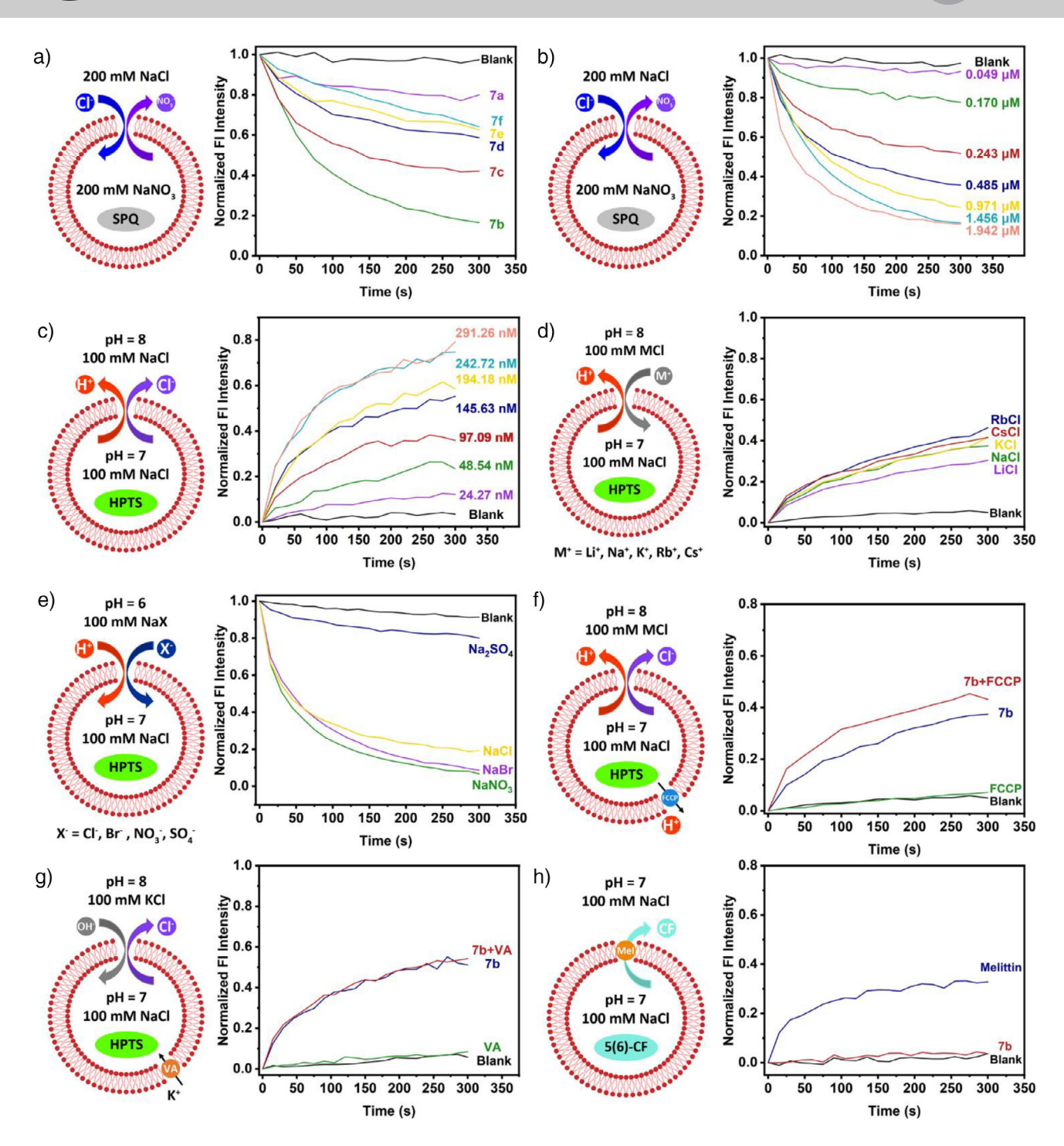


Figure 3. Anion transport studies with different azo-BU[6]s. a). Chloride transport activity in SPQ assay with 7a-7f (1.46 μM); b). Dose-dependent anion transport facilitated by 7b in SPQ assay and c) in HPTS assay; d) Cation transport (97.09 nM) and e) anion selectivity (24.27 nM) in HPTS assay with 7b; F. H $^+$ /Cl $^-$ symport (or the equivalent Cl $^-$ /OH $^-$ antiport) facilitated by 7b (97.09 nM) in the presence of FCCP (200 nM) in HPTS assay, comparing the transport rate between H $^+$ and Cl $^-$; G. H $^+$ /Cl $^-$ symport facilitated by 7b (97.09 nM) in the presence of valinomycin (200 pM) in HPTS assay, comparing the transport rate between OH $^-$ and Cl $^-$; H. Membrane integrity was assessed in the presence of 7b (97.09 nM) in the CF-leakage assay, with pore-forming protein Melittin (200 nM) used as a positive control.

surrounding solution contained sodium chloride. After adding the azo-BUs, we tracked the Cl⁻/NO₃⁻ exchange by monitoring chloride movement via changes in fluorescence over 5 min. Finally, detergent was added to break the vesicles and set the baseline signal.

As shown in Figure 3a, the transport activities of the (E)-isomers followed the order: 7b > 7c > 7d > 7e > 7f > 7a. This trend suggests that ion transport efficiency generally decreases with increasing alkyl chain length, except for compound 7a, which exhibits the lowest activity due to

15213773, 0. Downloaded from https://onlinelibrary.wiley.com/doi/10.1002/anie.202519101 by Hangzhou Normal University, Wiley Online Library on [10/11/2025]. See the Terms and Conditions (https://onlinelibrary.wiley.com/erms-and-conditions) on Wiley Online Library for rules of use; OA arctices are governed by the applicable Creative Commons Licenses

its rigid structure and poor solubility. To further investigate anion transport behavior, concentration-dependent Hill analysis was performed for each (E)-isomer to determine the half-maximal effective concentration (EC₅₀) for Cl⁻/NO₃⁻ exchange (Figures 3b and S34–S38). The resulting EC₅₀ values mirrored the activity trend observed in the fluorescence-based assay, with compound 7b exhibiting the highest transport efficiency. Specifically, 7b showed an EC₅₀ of 0.34 µM and a Hill coefficient (n) of 1.17, suggesting a 1:1 stoichiometry implying that a single transporter molecule mediates both anion uptake and release across the membrane. Due to its poor solubility, compound 7a was excluded from subsequent studies.

To further examine the H⁺/Cl⁻ symport (or the equivalent OH⁻/Cl⁻ antiport) mechanism facilitated by 7b, a fluorescence-based assay employing 8-hydroxypyrene-1,3,6trisulfonate (HPTS) was conducted (see SI). EYPC-based large LUVs were loaded with HPTS and NaCl, buffered to pH 7.0 with 4-(2-hydroxyethyl)-1-piperazineethanesulfonic acid (HEPES), and then suspended in an external NaCl solution buffered to pH 8.0, thereby creating a transmembrane pH gradient. Upon addition of 7b in DMSO, proton-coupled chloride transport was triggered, and the resulting dissipation of the pH gradient was tracked in real time. At the conclusion of the assay, vesicles were lysed with detergent to normalize fluorescence to its maximum intensity. The concentrationdependent transport activity and Hill analysis of 7b are presented in Figures 3c and S40. Furthermore, substituting extravesicular Na+ with Li+, K+, Rb+, or Cs+ resulted in minimal changes to transport efficiency, indicating that alkali metal cations do not play a direct role in the transport mechanism (Figures 3d and S41-S44). To evaluate anion selectivity, the external solution was replaced with Na⁺ salts containing various counter-anions (Cl-, Br-, NO₃-, or SO₄²⁻), buffered to pH 6.0 with HEPES. Variations in HPTS fluorescence decay across different anions revealed that the transport activity of azo-BUs is modulated by anion identity and generally aligns with the Hofmeister series (Figures 3e and \$45-\$48).

To clarify the intrinsic transport mechanism of azo-BUs, carbonyl cyanide 4-((trifluoromethoxy)phenylhydrazone) (FCCP), a well-known electrogenic protonophore, [56] was incorporated into HPTS assays alongside azo-BUs to probe their selectivity between Cl⁻ and H⁺. If azo-BUs preferentially transport Cl- over H+, FCCP should facilitate proton translocation, alleviating the rate-limiting step and enhancing overall transport efficiency. As expected, both the initial transport rates and overall Cl⁻ flux were markedly increased in the presence of FCCP, supporting a mechanistic preference for Cl⁻ over H⁺ (Figures 3f and S49-S52). Similarly, valinomycin (VA), a selective electrogenic K^+ carrier, was employed to evaluate the relative transport efficiency between Cl- and OH-. To establish a transmembrane pH and K+ gradient, the extravesicular solution was replaced with 100 mM KCl buffered at pH 8.0. Valinomycin-mediated K+ uniport into LUVs could then drive the influx of either Cl- or OH- via azo-BUs to maintain charge balance. If OH⁻ transport were more efficient than Cl⁻, a synergistic increase in transport activity would be

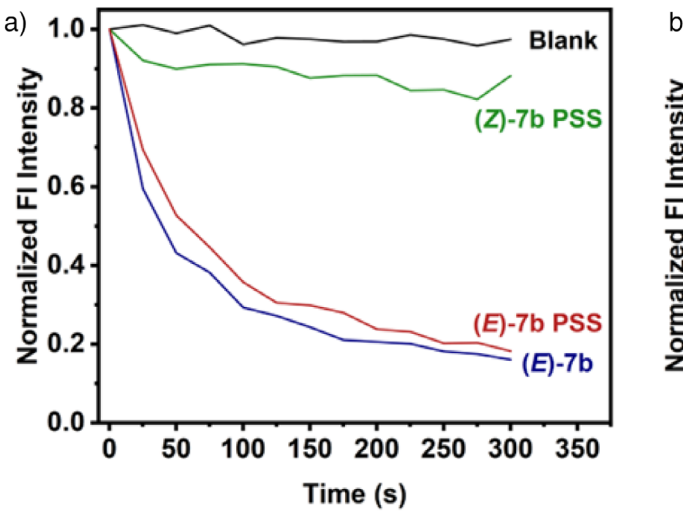
expected upon VA addition. However, no such enhancement was observed, indicating that Cl- transport is favored over OH⁻ (Figures 3g and S53–S56).

Membrane integrity was further assessed using a 5(6)carboxyfluorescein (CF) leakage assay.^[57] In this assay, CF remains self-quenched within intact LUVs and fluoresces upon release through membrane disruption. As a positive control, the pore-forming peptide melittin triggered a pronounced increase in fluorescence, confirming membrane permeabilization. In contrast, treatment with transporter 7b resulted in no detectable leakage, indicating that the membrane remained structurally intact in the presence of 7b (Figure 3h). This observation is corroborated by dynamic light scattering (DLS) analysis, which showed no significant changes in vesicle size or distribution (Figure S71).

Together with the CF leakage and DLS analyses, the fatty acid flip-flop mechanism was investigated to further probe the membrane interaction profile of azo-BUs. This mechanism, previously reported for acyclic thiourea transporters, [58,59] was assessed using a tetrabutylammonium hydroxide (TBAOH) assay, [60] which selectively detects electrogenic H⁺/OH⁻ transport (Figure S57). As anticipated, the assay confirmed the protonophoric activity of FCCP and thiourea 8, validating the method's sensitivity. In contrast, all azo-BUs exhibited no activity under these conditions, indicating a lack of electrogenic proton transport (Figures S58–S64). This inactivity may stem from steric hindrance and the inherently soft character of the C-H bond, which is insufficiently acidic to engage in effective binding with the fatty acid carboxylate head group. Building on the absence of electrogenic proton transport, we next explored whether azo-BUs could facilitate chloride transport via electrogenic or electroneutral pathways. Given that certain anion transporters are known to mediate both modes, a cationophore-coupled assay was employed to distinguish between them (Figure S65). In this setup, LUVs preloaded with SPQ and buffered potassium gluconate (KGlu) were suspended in an external KCl solution, and real-time Cl⁻ influx was monitored. The chloride gradient served as the driving force, while gluconate, being large and hydrophilic, acted as a non-permeable counterion, minimizing its influence on transport dynamics. Notably, chloride influx mediated by azo-BUs was markedly enhanced in the presence of valinomycin, a K⁺-selective electrogenic carrier, compared to monensin, an electroneutral K⁺/H⁺ exchanger. These findings indicate that azo-BUs predominantly operate via an electrogenic chloride transport mechanism (Figures S66–S70), further distinguishing their functional profile from classical protonophores and thiourea-based systems.

Reversible Photo-Switchable Anion Transport

To further characterize the functional versatility of azo-BUs, we investigated their reversible photo-switchable anion transport properties using SPQ-based assays in LUVs. Building on their electrogenic chloride transport behavior, these experiments probed how light-induced isomerization modulates activity. Prior to each measurement, samples were irradiated with either 365 or 450 nm light to establish the corresponding



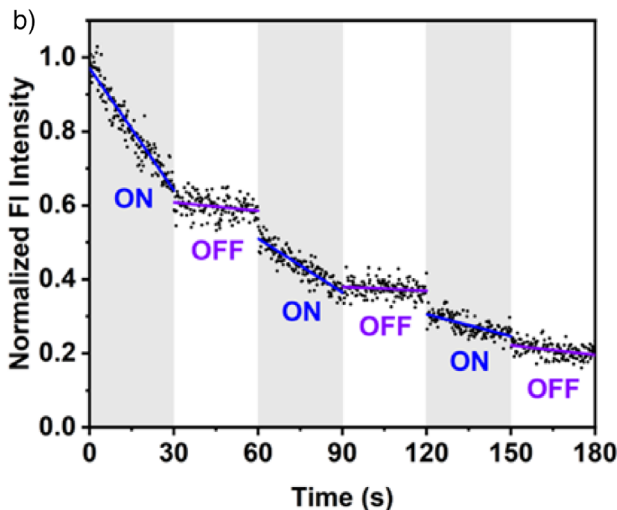


Figure 4. Light-controlled modulation of chloride transport by azo-BU 7b. a). SPQ assay results showing the ion transport activity of (E)-7b (1.46 μM), the PSS of (Z)-7b obtained under 365 nm irradiation, and the PSS of (E)-7b obtained under 450 nm irradiation, and b). Real-time ON–OFF–ON-OPF–ON- photo-switching cycles demonstrating reversible control of Cl⁻ transport across the membrane. Irradiation at 365 nm for 5 s (OFF) and 450 nm for 3 s (ON) enabled precise toggling between inactive and active states. Data acquisition was briefly paused during each irradiation and resumed immediately, introducing only negligible error. Purple and blue lines represent linear fits to the transport kinetics.

PSS. Across all compounds, the (E)-isomers consistently exhibited markedly higher transport activity than their (Z)isomer counterparts generated under 365 nm irradiation (Figure S72). Among them, (E)-7b stood out, demonstrating a Cl- transport efficiency nearly sevenfold greater than its (Z)-form at 1.46 µM (Figure 4a). Importantly, 7b retained robust and reversible transport performance under repeated cycles of alternating 365 and 450 nm irradiation, with no discernible loss in activity (Figure \$73). Other azo-BUs, including 7f, the longest in molecular length, also displayed clear ON/OFF switching behavior in the LUV assay (Figure S74). This behavior suggests that the diminished activity of the (Z)-isomer is not due to geometric constraints preventing membrane spanning or ion pathway formation, as seen in machine-like transporter relays.[21] Instead, consistent with previous findings,[51] the photo-switchable behavior likely arises from changes in molecular polarity induced by E-Z isomerization, which modulate membrane affinity and transport efficiency. Although the results emphasize reduced membrane insertion for the (Z)-isomers, we acknowledge that alternative mechanisms, such as a photo-induced block effect, [61] where the isomer remains membrane-associated but sterically hinders ion conduction, cannot be ruled out at this stage.

To further validate the reversible photo-switching capability of azo-BUs, we performed a series of ON \rightarrow OFF and OFF \rightarrow ON cycles, focusing on the Cl⁻ transport activity of compound **7b** using the SPQ assay (Figures 4b and S76). Building on the robust light-responsive behavior previously observed, alternating irradiation at 365 and 450 nm enabled precise toggling between the active (ON) and inactive (OFF) states. This dynamic control closely resembles the light-regulated gating mechanisms found in natural ion channel proteins. Remarkably, the ON state of **7b** exhibited an average transport rate 33 times greater than the OFF state, with peak

differences approaching a 200-fold increase (Tables S1 and S2). These results underscore the efficiency and reliability of **7b** as a photo-switchable anion transporter, capable of sustained and reversible modulation under light stimuli.

To ensure that the observed photo-switchable transport was indeed attributable to azobenzene isomerization and not an artifact of light exposure, control experiments were conducted. Vesicles lacking compound 7b showed no detectable ion permeation following 365 nm irradiation for 300 s, confirming that the structural integrity of the lipid bilayer remains unaffected by light alone (Figure S77). Additionally, a non-photo-responsive semiaza-BU[6] derivative (compound 9) exhibited no switching behavior under identical conditions, underscoring the essential role of azobenzene photoisomerization in enabling light-controlled ion transport (Figure \$78). Supporting this, UV-vis absorption spectra and photochemical cycling studies of 7b embedded in vesicles revealed behavior nearly identical to that observed in solution, even under repeated irradiation at 365 and 450 nm (Figures S79 and S80). Collectively, these findings confirm that the reversible transport activity of azo-BUs is governed by E-Z isomerization of the azobenzene units, providing a robust platform for light-regulated membrane transport.

Inspired by natural light-responsive transporter proteins such as the anion pump halorhodopsin^[62] and anion channel rhodopsin,^[63] which regulate chloride flux across membranes to modulate cellular polarization, we investigated the capacity of **7b** to modulate membrane potential in a liposome model using the voltage-sensitive dye Safranin O.

In the polarization assay, LUVs loaded with buffered potassium glutamate (KGlu) were suspended in an external NaCl buffer (pH 7.0). Upon addition of **7b**, chloride influx into the vesicles triggered membrane polarization, as the impermeable glutamate anions remained confined within the lumen (Figure S81). For the depolarization assay, LUVs

vnloaded from https://onlinelibrary.wiley.com/doi/10.1002/anie.202319101 by Hangzhou Normal University, Wiley Online Library on [10/11/2025]. See the Terms and Conditions (https://onlinelibrary.wiley.com/terms-and-conditions) on Wiley Online Library for rules of use; OA articles are governed by the applicable Creative Commons Licensed

·100 mV

Research Article

 $= 89.4 \pm 2.8 pS$

15213773, Q. Downloaded from https://onlinelibrary.wiley.com/doi/10.1002/anie.202519101 by Hangzhou Normal University, Wiley Online Library on [10/11/2025]. See the Terms and Conditions (https://onlinelibrary.wiley.com/terms-and-conditions) on Wiley Online Library for rules of use; OA articles are governed by the applicable Creative Commons

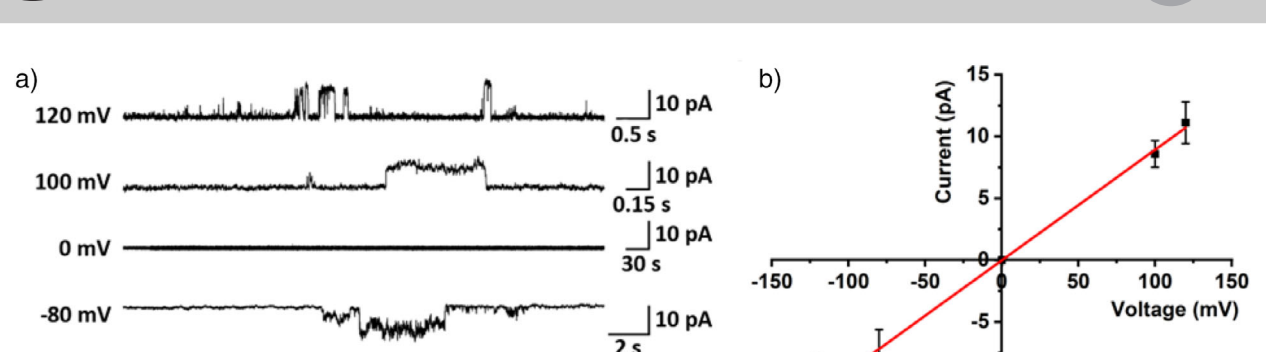


Figure 5. Single-channel recordings and I-V analysis of azo-BU[6] 7b. a) Representative current traces across various applied voltages; b) fitted I-V plot showing chloride ion conductance. Data are presented as mean \pm standard deviation (SD).

____ 10 pA

were instead filled with KCl under identical buffer conditions. Introduction of the electrogenic potassium carrier VA facilitated K^+ efflux, generating a positive membrane potential. Subsequent chloride influx mediated by **7b** counterbalanced this potential, leading to membrane depolarization (Figure S82). These experiments reveal that the (E)-isomer of **7b** effectively drives both polarization and depolarization of membrane potential, while the (Z)-isomer exerts only a negligible effect. This light-dependent behavior underscores the utility of **7b** as a molecular tool for reversible, photocontrolled modulation of membrane potential.

Ion Channel Mechanism

Typically, ion transport by carriers across 1,2-dihexadecanoylrac-glycero-3-phosphocholine (DPPC) vesicle membranes is minimal at room temperature and only becomes active above the membrane's phase transition point. [18] Interestingly, (E)-7b showed measurable transport activity even at ambient conditions (Figure \$83), suggesting it may operate via a single-molecule channel mechanism. To investigate this, the channel-like behavior of (E)-7b was examined using planar bilayer membranes made from 1,2-diphytanoyl-sn-glycero-3-phosphocholine (DiPhyPC) lipids (Figure S84).^[64] When both sides of the membrane contained 1.0 M KCl, consistent patterns of channel opening and closing were observed across voltages from -100 to 120 mV (Figure 5a). The resulting current-voltage data showed a chloride ion conductance of 89.4 ± 2.8 pS, based on four independent trials (Figure 5b). These results strongly support that (E)-7b enables ion movement through a channel-like pathway rather than acting as a mobile carrier. Notably, no transport activity was detected at -80 mV with (Z)-7b unless the system was irradiated with 450 nm light (Figure \$85), confirming that chloride transport can be switched on by light.

Cell Viability

Synthetic ion transporters can disrupt cellular homeostasis by facilitating transmembrane ion flux, particularly through excessive chloride influx. This dysregulation of intracellular ion balance is often associated with impaired cellular function and the activation of cell death pathways.[57,65-70] Building on the efficient and light-controllable ion transport observed in liposomal models, the potential of azo-BUs as anticancer agents was also investigated. Among the candidates, (E)-7b demonstrated the highest transport activity and was selected for further evaluation of its cytotoxic properties and mechanism of action. Cytotoxicity was assessed using the Cell Counting Kit-8 (CCK-8) assay across three cancer cell lines: human non-small cell lung carcinoma (A549), murine melanoma (B16), and human glioblastoma (U-87 MG). Following 24 h of co-incubation, (E)-7b induced marked cytotoxicity in all cell lines, with the most pronounced effect observed in U-87 MG cells (IC₅₀ = 5.65 μ M) (Figures 6a and S86). Based on these results, subsequent mechanistic studies were focused on U-87 MG cells.

-15

To assess the differential cytotoxicity of the E/Z isomers of azo-BU[6] 7b, cell viability was measured across a range of concentrations for both (E)-7b and (Z)-7b. The results closely mirrored those observed in liposomal transport studies: (E)-7b exhibited significant cytotoxicity, in contrast to the markedly lower toxicity observed with (Z)-7b. This marked contrast underscores the potential of photo-responsive azo-BUs as tunable agents for cancer therapy (Figure 6b). Subsequently, we examined the potential for in situ modulation of ion transport activity within live cell systems. Following a 2 h incubation with cells, (E)-7b was effectively photo-isomerized to its less toxic (Z)-form via 365 nm light irradiation for 10 min. Continued incubation for an additional 22 h led to a marked preservation of cell viability. Similarly, cells treated with (Z)-7b under identical conditions exhibited no cytotoxic response (Figure 6c). Microscopic examination of the cells revealed visible precipitation, likely attributable to the reduced membrane permeability of (Z)-7b following its polarity shift (Figure S87).[71] To mitigate precipitation and improve cellular uptake, the pre-incubation time for (Z)-7b was reduced to 10 min, followed by 10 min of irradiation with 450 nm light and a subsequent 24 h incubation. The CCK-8 assay confirmed restored cytotoxicity, indicating that (Z)-7b is capable of undergoing effective photoisomerization within cellular systems (Figure \$88) and confirming that the

15213773, 0. Downloaded from https://onlinelibrary.wiley.com/doi/10.1002/aniec.202519101 by Hangzhou Normal University, Wiley Online Library on [10/11/2025]. See the Terms and Conditions (https://onlinelibrary.wiley.com/

and-conditions) on Wiley Online Library for rules of use; OA articles are governed by the applicable Creative Commons

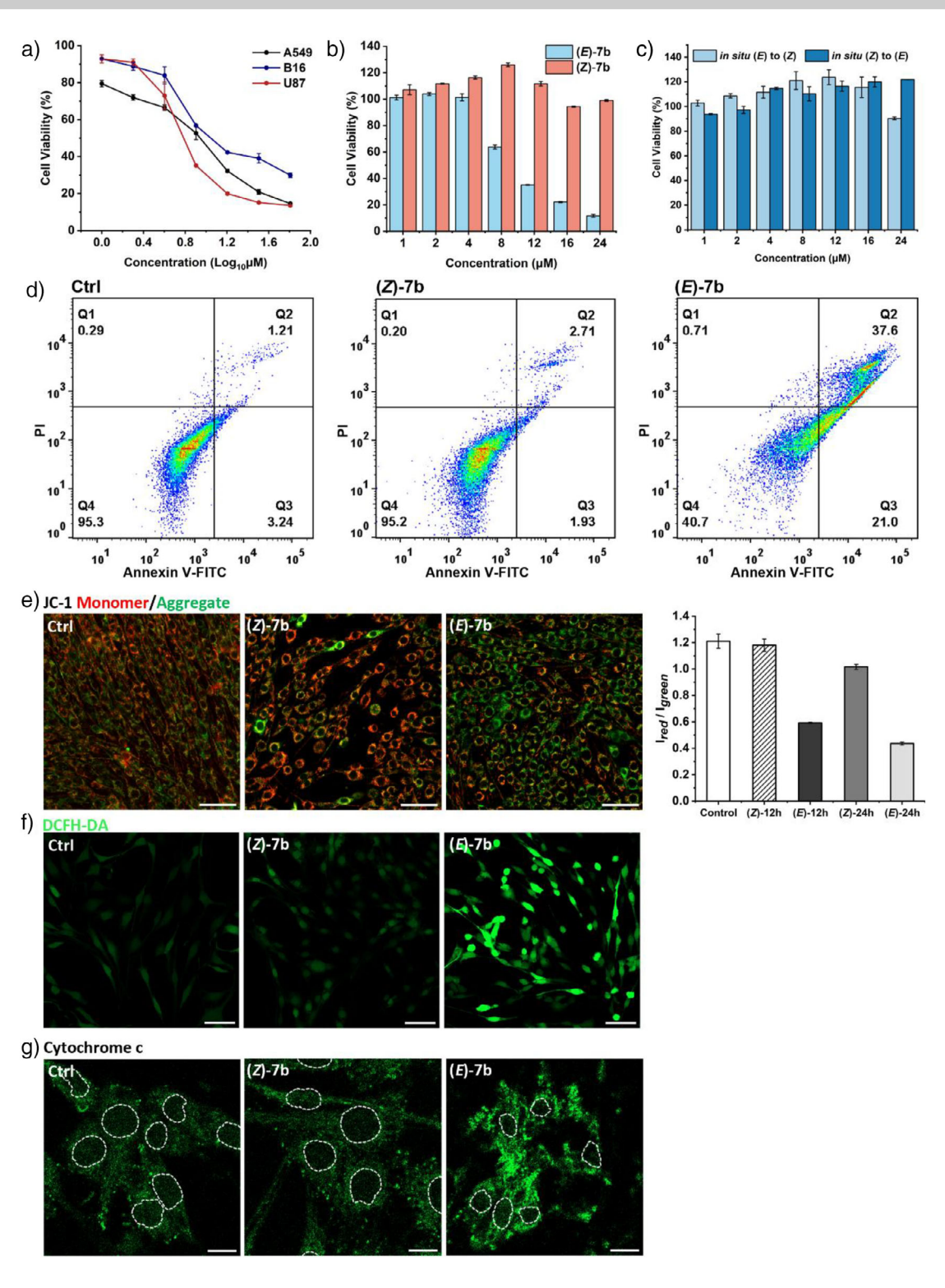


Figure 6. a) Dose-dependent cytotoxicity of 7b in A549, B16, and U-87 MG cells for 24 h incubation. Cellular viability was assessed using the CCK-8 assay; b) Cell viability of U-87 MG cells following 24 h incubation with (E)-7b and (Z)-7b. Each data point represents the average of three measurements, with the error bars indicating SD; c) Cell viability of (E)-7b and (Z)-7b after in situ photoisomerization under light irradiation. Each data point represents the average of three measurements, with the error bars indicating SD; d) Flow cytometry analysis of U-87 MG cells treated with 20 μM of (E)-7b and (Z)-7b for 24 h, stained with fluorescein-annexin V and PI. Untreated cells served as a negative control; e) Cell imaging of U-87 MG cells treated with (E)-7b and (E)-7b for 12 h, stained with JC-1. JC-1 aggregates are shown in red, and JC-1 monomers are shown in green. DMSO was used as a control. Scale bar = 50 μm. Quantitative analysis of the ratio of red and green fluorescence. Data are presented as mean ± SD; f) Cell imaging of U-87 MG cells treated with (E)-7b and (E)-7b for 24 h, stained with DCFH-DA. DMSO was used as a control. Scale bar = 50 μm; g) Cell imaging of U-87 MG cells treated with (E)-7b and (E)-7b for 24 h, showing the distribution of cytochrome c signals. White dashed circles represented the boundaries of the nucleus. Scale bar = 10 μm.

lack of effect in Figure 6c was largely procedural rather than mechanistic.

To investigate the mechanism underlying cell death, cells were incubated with (E)-**7b** for 24 h. As a negative control, a parallel set of cells was treated with (Z)-**7b**. Post-treatment, cells were stained with fluorescein-conjugated annexin V and propidium iodide (PI), followed by flow cytometric analysis to quantify apoptotic populations. In comparison to the untreated control, treatment with (E)-**7b** significantly increased the proportion of cells undergoing early and late apoptosis to 21.0% and 37.6%, respectively. By contrast, treatment with (Z)-**7b** yielded only 4.64% apoptotic cells, closely aligning with the baseline level observed in the untreated group (4.45%) (Figure 6d). These results demonstrate that (E)-**7b** induces apoptosis, whereas (Z)-**7b** does not, highlighting the potent and selective photo-switchable anticancer activity of compound **7b**.

Loss of mitochondrial membrane potential (MMP) is a well-established hallmark of apoptosis. To evaluate MMP disruption, a membrane-potential-sensitive fluorescent probe (JC-1) was employed. In healthy mitochondria, the probe accumulates and forms red-fluorescent J-aggregates. Upon MMP depolarization, the probe dissociates into monomeric forms that redistribute into the cytosol, emitting green fluorescence. As shown in Figure 6e, treatment with (E)-7b led to a pronounced reduction in red fluorescence accompanied by a corresponding increase in green fluorescence, consistent with apoptotic induction. Quantitative analysis revealed a timedependent decline in the red-to-green fluorescence intensity ratio (I_{red}/I_{green}) following exposure to (E)-7b for 12 and 24 h. By comparison, (Z)-7b elicited only a marginal change in this ratio (Figures 6e, S89, and S90). These findings confirm that (E)-7b disrupts MMP, whereas (Z)-7b exerts minimal effects, aligning with its low cytotoxic profile.

Following the observed depolarization of MMP by (E)-7b, we investigated its downstream consequences, specifically the induction of oxidative stress and the accumulation of reactive oxygen species (ROS). Mitochondrial dysfunction is known to elevate cytosolic ROS levels, which play a pivotal role in initiating apoptotic signaling. To quantify ROS production, cells treated with (E)-7b or (Z)-7b were incubated with the fluorescent probe 2',7'-dichlorodihydrofluorescein diacetate (DCFH-DA). Fluorescence intensity in (Z)-7b-treated cells remained comparable to that of the untreated control, indicating minimal ROS generation.

In contrast, treatment with (*E*)-**7b** elicited pronounced green fluorescence, consistent with substantial ROS accumulation (Figure 6f). Excessive ROS can trigger the opening of mitochondrial permeability transition pores (mPTP), facilitating the release of cytochrome c into the cytosol, a hallmark of intrinsic apoptosis. To assess this event, U-87 MG cells were immunostained with a cytochrome c-specific antibody. Compared to both the untreated and (*Z*)-**7b**-treated groups, cells exposed to (*E*)-**7b** exhibited a marked increase in cytosolic green fluorescence, indicating cytochrome c translocation (Figure 6g). Together with the MMP and ROS data, these findings strongly support the conclusion that (*E*)-**7b** induces apoptosis via mitochondrial disruption and oxidative stress,

whereas (Z)-7b remains biologically inert under identical conditions.

Following the observation of (E)-7b's chloride transport activity and its involvement in apoptosis, we next examined whether this compound also perturbs lysosomal pH, a key regulator of cellular homeostasis and enzymatic function. To assess chloride ion influx by 7b, U-87 MG cells were stained with the membrane-permeable, chloride ion-sensitive fluorescent probe N-(ethoxycarbonylmethyl)-6-methoxyquinolinium bromide (MQAE) and imaged in real time using a confocal laser scanning microscope. As shown in Figure 7a, cells treated with (E)-7b exhibited markedly reduced fluorescence intensity compared to the other two groups within the same experimental time frame. This pronounced quenching effect is consistent with enhanced intracellular chloride accumulation, indicative of elevated intracellular chloride levels. This pronounced quenching effect supports the hypothesis of enhanced chloride accumulation. Moreover, 7b showed a pronounced impact on lysosomes, suggesting that part of the uptake may occur through endocytosis. However, due to the synthetic constraints of azo-BUs, we were unable to introduce a fluorescent tag for direct localization studies.

Beyond its role in cytosolic chloride accumulation, (E)-7b may also exert cytotoxic effects by disrupting lysosomal acidification, a process essential for cellular homeostasis. The luminal acidic environment of lysosomes (pH < 5.0) is critical for the optimal activity of resident hydrolytic enzymes. This acidity is sustained through the coordinated action of the ClC-7 chloride/proton antiporter and the vacuolar-type H⁺-ATPase (V-ATPase), and is closely linked to the intralysosomal chloride concentration, which typically reaches ~80 mM.^[72-74] To date, only a limited number of synthetic ion transporters have been reported to induce apoptosis via disruption of lysosomal pH homeostasis.[66,67,75-77] Given the intrinsic H⁺/Cl⁻ cotransport capability of azo-BUs, it is hypothesized that these compounds facilitate HCl efflux from lysosomes, resulting in pH neutralization, collapse of ionic and proton gradients, impairment of lysosomal enzymatic function, and ultimately, enhanced cytotoxicity.

To experimentally validate this hypothesis, we employed Lysotracker Deep Green, a pH-sensitive fluorescent dye that preferentially accumulates in acidic intracellular compartments. Under neutral or basic conditions, its fluorescence is markedly diminished or absent. Based on this principle, U-87 MG cells were treated with 7b for 30 min and subsequently stained with Lysotracker Deep Green to assess lysosomal pH modulation. As shown in Figure 7b, treatment with (E)-7b resulted in a pronounced decrease in fluorescence intensity, indicating substantial lysosomal deacidification. In contrast, cells treated with (Z)-7b exhibited only a modest reduction in fluorescence relative to the untreated control, likely attributable to residual (E)-isomer present in the PSS of (Z)-7b. Moreover, (E)-7b maintained consistent chloride ion transport activity at both pH 4.0 and 7.2, confirming its functional stability within the acidic lysosomal environment (Figure \$39).

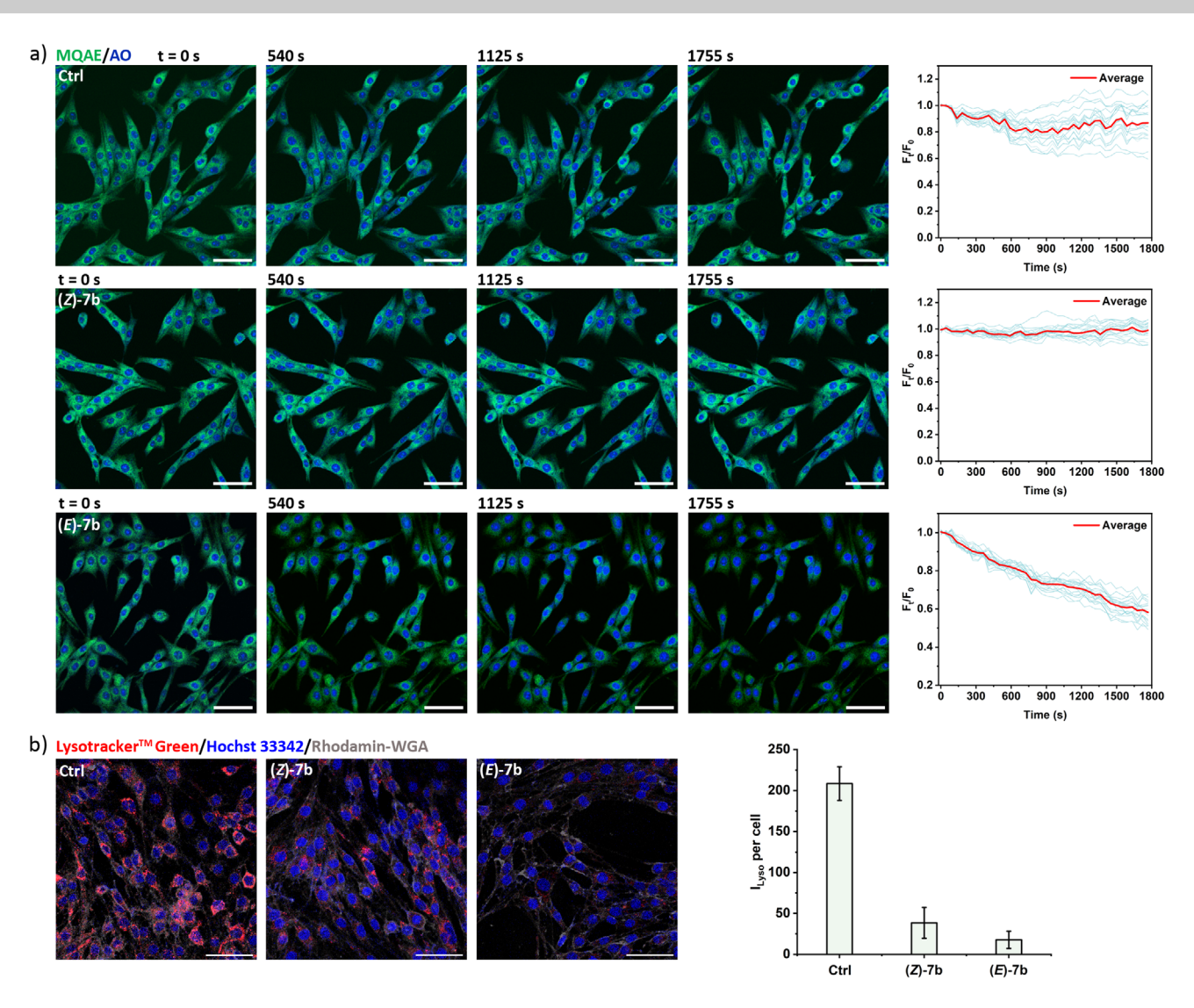


Figure 7. a) Cell imaging of U-87 MG cells treated with (E)-7b and (Z)-7b at different time points. The nucleus was stained with AO. MQAE was shown in green and AO in blue. DMSO was used as a control. Scale bar $= 50 \mu m$; b) cell imaging of U-87 MG treated with (E)-7b and (Z)-7b for 30 min, stained with Lysotracker Green (shown in red). The nucleus was stained with Hoechst 33 342 (shown in blue), and the cell membrane was stained with rhodamine-labeled wheat germ agglutinin (shown in grey). DMSO was used as a control. Scale bar $= 50 \mu m$. Data are presented as mean \pm SD.

Conclusion

We have demonstrated that azo-functionalized bambusuril derivatives (azo-BUs) undergo reversible photoisomerization between (E)- and (Z)-configurations, enabling dynamic light-controlled modulation of chloride transport activity. Among the derivatives examined, compound (E)-7b consistently exhibits the highest transport efficiency, which can be switched off upon irradiation with 365 nm light and reactivated upon exposure to 450 nm light. Mechanistic studies, including cationophore-coupled assays and planar bilayer recordings, confirm that (E)-7b mainly mediates chloride transport via an electrogenic pathway. Notably, its single-molecule channel-like behavior sets it apart from conventional mobile carriers, suggesting a distinct mode of membrane interaction. Despite robust ion transport, (E)-7b does not disrupt membrane integrity, as evidenced by CF

leakage and DLS assays. It selectively transports Cl^- over H^+ and OH^- , with activity modulated by anion identity in accordance with the Hofmeister series.

Cellular cytotoxicity and apoptosis experiments reveal that (E)-7b induces significant cytotoxicity in multiple cancer cell lines, especially U-87 MG glioblastoma cells. Its cytotoxicity is light-tunable, with the (Z)-isomer showing minimal toxicity. Mechanistic studies indicate that (E)-7b induces apoptosis through the disruption of MMP, ROS accumulation, and cytochrome c release. Importantly, (E)-7b also disrupts lysosomal acidification via H^+/Cl^- co-transport, impairing enzymatic function and contributing to cytotoxicity. These findings highlight the dual role of (E)-7b in perturbing both cytosolic and lysosomal ion homeostasis, and underscore its promise as a photo-switchable therapeutic agent. This dual perturbation of cytosolic and lysosomal ion homeostasis underscores the compound's multifaceted

vnloaded from https://onlinelibrary.wiley.com/doi/10.1002/anie.2025/19101 by Hangzhou Normal University, Wiley Online Library on [10/11/2025]. See the Terms and Conditions (https://onlinelibrary.wiley.com/terms-and-conditions) on Wiley Online Library for rules of use; OA articles are governed by the applicable Creative Commons

15213773, 0. Downloaded from https://onlinelibrary.wiley.com/doi/10.1002/anie.202519101 by Hangzhou Normal University, Wiley Online Library on [10/11/2025]. See the Terms and Conditions (https://onlinelibrary.wiley.com/terms-and-conditions) on Wiley Online Library for rules of use; OA articles are governed by the applicable Creative Commons



cytotoxic mechanism. The ability to control transport activity with light positions azo-BUs as promising candidates for the development of next-generation, stimuli-responsive anticancer agents.

Supporting Information

The data supporting the findings of this study are available in the Supporting Information of this article.

Acknowledgements

This work was supported by the National Natural Science Foundation of China (Nos. 22275046), the National Key R&D Program of China (No. 2020YFA0908500) and the Hangzhou Leading Innovation and Entrepreneurship Team Project (TD2022001) and the Interdisciplinary Research Project of Hangzhou Normal University (2024JCXK01) and the Science and Technology Development Planning Project of Jilin Province (No. YDZJ202301ZYTS300). L. He thanks Dr. Dingcheng Zhu for guidance on cell experiments and confocal laser scanning microscopy techniques. O. Reany thanks the financial support of ISF-NSFC joint research program grant (3665/21) for the collaborative project.

Conflict of Interests

The authors declare no conflict of interest.

Data Availability Statement

The data that support the findings of this study are available in the Supporting Information of this article.

Keywords: Apoptosis • Azo-functionalized bambusurils • Light-responsive ion channel • Photo-switchable chloride transporter • Reversible photoisomerization

- D. C. Gadsby, Nat. Rev. Mol. Cell Biol. 2009, 10, 344–352, https://doi.org/10.1038/nrm2668.
- [2] G. M. Cooper, *The Cell: A Molecular Approach*, Oxford University Press, Oxford **2018**.
- [3] H. E. Kato, F. Zhang, O. Yizhar, C. Ramakrishnan, T. Nishizawa, K. Hirata, J. Ito, Y. Aita, T. Tsukazaki, S. Hayashi, P. Hegemann, A. D. Maturana, R. Ishitani, K. Deisseroth, O. Nureki, *Nature* 2012, 482, 369–374.
- [4] S. P. H. Alexander, A. Mathie, J. A. Peters, Br. J. Pharmacol. 2011, 164, S115–S135.
- [5] H. Yeo, V. Mehta, A. Gulati, D. Drew, *Nature* 2023, 623, 193–201, https://doi.org/10.1038/s41586-023-06518-2.
- [6] Y. Ramu, Y. Xu, Z. Lu, *Nature* 2006, 442, 696–699, https://doi. org/10.1038/nature04880.
- [7] P. A. Gottlieb, F. Sachs, *Nature* 2012, 483, 163–164, https://doi. org/10.1038/483163a.
- [8] H. Kandori, K. Inoue, S. P. Tsunoda, Chem. Rev. 2018, 118, 10646–10658.

- [9] T. Weinert, P. Skopintsev, D. James, F. Dworkowski, E. Panepucci, D. Kekilli, A. Furrer, S. Brünle, S. Mous, D. Ozerov, P. Nogly, M. Wang, J. Standfuss, *Science* 2019, 365, 61–65, https://doi.org/10.1126/science.aaw8634.
- [10] S. Mous, G. Gotthard, D. Ehrenberg, S. Sen, T. Weinert, P. J. M. Jonhson, D. James, K. Nass, A. Furrer, D. Kekilli, P. Ma, S. Brünle, C. M. Casadei, I. Maretiel, F. Dworkowski, D. Gashi, P. Skopintsev, M. Wranik, G. Knopp, E. Panepucci, V. Panneels, C. Cirelli, D. Ozerov, G. F. X. Schertler, M. Wang, C. Milne, J. Standfuss, I. Schapiro, J. Heberle, P. Nogly, *Science* 2022, 375, 845–851.
- [11] T. Muraoka, K. Umetsu, K. V. Tabata, T. Hamada, H. Noji, T. Yamashita, K. Kinbara, J. Am. Chem. Soc. 2017, 139, 18016–18023, https://doi.org/10.1021/jacs.7b09515.
- [12] X. Wu, J. R. Small, A. Cataldo, A. M. Withecombe, P. Turner, P. A. Gale, *Angew. Chem. Int. Ed.* 2019, 58, 15142–15147, https://doi.org/10.1002/anie.201907466.
- [13] M. Fares, X. Wu, D. Ramesh, W. Lewis, P. A. Keller, E. N. W. Howe, R. Pérez-Tomás, P. A. Gale, *Angew. Chem., Int. Ed.* 2020, 59, 17614–17621, https://doi.org/10.1002/anie.202006392.
- [14] S.-P. Zheng, J.-J. Jiang, A. van der Lee, M. Barboiu, Angew. Chem., Int. Ed. 2020, 59, 18920–18926.
- [15] W.-L. Huang, X.-D. Wang, Y.-F. Ao, Q.-Q. Wang, D.-X. Wang, Angew. Chem., Int. Ed. 2023, 62, e202302198, https://doi.org/10. 1002/anie.202302198.
- [16] J.-F. Lin, X.-D. Wang, Y.-F. Ao, Q.-Q. Wang, D.-X. Wang, Angew. Chem., Int. Ed. 2024, 63, e202411702, https://doi.org/10.1002/anie.202411702.
- [17] L. Shi, W. Zhao, Z. Jiu, J. Guo, Q. Zhu, Y. Sun, B. Zhu, J. Chang, P. Xin, Angew. Chem., Int. Ed. 2024, 63, e202403667, https://doi. org/10.1002/anie.202403667.
- [18] A. Kerckhoffs, M. J. Langton, Chem. Sci. 2020, 11, 6325–6331, https://doi.org/10.1039/D0SC02745F.
- [19] S. J. Wezenberg, L.-J. Chen, J. E. Bos, B. L. Feringa, E. N. W. Howe, X. Wu, M. A. Siegler, P. A. Gale, J. Am. Chem. Soc. 2022, 144, 331–338, https://doi.org/10.1021/jacs.1c10034.
- [20] L. E. Bickerton, M. J. Langton, Chem. Sci. 2022, 13, 9531–9536, https://doi.org/10.1039/D2SC03322D.
- [21] T. G. Johnson, A. Sadeghi-Kelishadi, M. J. Langton, J. Am. Chem. Soc. 2022, 144, 10455–10461, https://doi.org/10.1021/jacs. 2c02612
- [22] M. Ahmad, T. G. Johnson, M. Flerin, F. Duarte, M. J. Langton, Angew. Chem., Int. Ed. 2024, 63, e202403314, https://doi.org/10. 1002/anie.202403314.
- [23] E. Grählert, M. J. Langton, Angew. Chem., Int. Ed. 2024, n/a, e202421580.
- [24] J. T. Davis, P. A. Gale, O. A. Okunola, P. Prados, J. C. Iglesias-Sánchez, T. Torroba, R. Quesada, *Nat. Chem.* 2009, 1, 138–144, https://doi.org/10.1038/nchem.178.
- [25] N. Busschaert, M. Wenzel, M. E. Light, P. Iglesias-Hernández, R. Pérez-Tomás, P. A. Gale, J. Am. Chem. Soc. 2011, 133, 14136– 14148, https://doi.org/10.1021/ja205884y.
- [26] N. Busschaert, I. L. Kirby, S. Young, S. J. Coles, P. N. Horton, M. E. Light, P. A. Gale, *Angew. Chem.*, *Int. Ed.* **2012**, *51*, 4426–4430
- [27] T. Saha, A. Gautam, A. Mukherjee, M. Lahiri, P. Talukdar, J. Am. Chem. Soc. 2016, 138, 16443–16451, https://doi.org/10.1021/jacs.6b10379.
- [28] T. Saha, M. S. Hossain, D. Saha, M. Lahiri, P. Talukdar, J. Am. Chem. Soc. 2016, 138, 7558–7567, https://doi.org/10.1021/jacs. 6b01723.
- [29] A. J. Plajer, J. Zhu, P. Pröhm, F. J. Rizzuto, U. F. Keyser, D. S. Wright, J. Am. Chem. Soc. 2020, 142, 1029–1037, https://doi.org/10.1021/jacs.9b11347.
- [30] A. V. Jentzsch, D. Emery, J. Mareda, S. K. Nayak, P. Metrangolo, G. Resnati, N. Sakai, S. Matile, *Nat. Commun.* 2012, 3, 905, https://doi.org/10.1038/ncomms1902.

ownloaded from https://onlinelibrary.wiley.com/doi/10.1002/anie.202319101 by Hangzhou Normal University, Wiley Online Library on [10/1/2025]. See the Terms and Conditions (https://onlinelibrary.wiley.com/cerms

and-conditions) on Wiley Online Library for rules of use; OA articles are governed by the applicable Creative Commons

- [31] H. M. Tay, T. G. Johnson, A. Docker, M. J. Langton, P. D. Beer, Angew. Chem., Int. Ed. 2023, 62, e202312745.
- [32] S. Benz, M. Macchione, Q. Verolet, J. Mareda, N. Sakai, S. Matile, J. Am. Chem. Soc. 2016, 138, 9093–9096, https://doi.org/10.1021/jacs.6b05779.
- [33] A. Docker, T. G. Johnson, H. Kuhn, Z. Zhang, M. J. Langton, J. Am. Chem. Soc. 2023, 145, 2661–2668, https://doi.org/10.1021/ jacs.2c12892.
- [34] L. M. Lee, M. Tsemperouli, A. I. Poblador-Bahamonde, S. Benz, N. Sakai, K. Sugihara, S. Matile, J. Am. Chem. Soc. 2019, 141, 810–814, https://doi.org/10.1021/jacs.8b12554.
- [35] M. Lisbjerg, H. Valkenier, B. M. Jessen, H. Al-Kerdi, A. P. Davis, M. Pittelkow, J. Am. Chem. Soc. 2015, 137, 4948–4951, https://doi.org/10.1021/jacs.5b02306.
- [36] P. Xin, H. Kong, Y. Sun, L. Zhao, H. Fang, H. Zhu, T. Jiang, J. Guo, Q. Zhang, W. Dong, C.-P. Chen, *Angew. Chem., Int. Ed.* 2019, 58, 2779–2784, https://doi.org/10.1002/anie.201813797.
- [37] S.-H. Park, I. Hwang, D. A. McNaughton, A. J. Kinross, E. N. W. Howe, Q. He, S. Xiong, M. D. Kilde, V. M. Lynch, P. A. Gale, J. L. Sessler, I. Shin, *Chem* 2021, 7, 3325–3339, https://doi.org/10.1016/j.chempr.2021.08.018.
- [38] P. Xin, L. Xu, W. Dong, L. Mao, J. Guo, J. Bi, S. Zhang, Y. Pei, C.-P. Chen, *Angew. Chem.*, *Int. Ed.* 2023, 62, e202217859, https://doi.org/10.1002/anie.202217859.
- [39] R. Cao, R. B. Rossdeutcher, Y. Zhong, Y. Shen, D. P. Miller, T. A. Sobiech, X. Wu, L. S. Buitrago, K. Ramcharan, M. I. Gutay, M. F. Figueira, P. Luthra, E. Zurek, T. Szyperski, B. Button, Z. Shao, B. Gong, *Nat. Chem.* 2023, 15, 1559–1568, https://doi.org/10.1038/s41557-023-01315-w.
- [40] Y.-H. Fu, Y.-F. Hu, T. Lin, G.-W. Zhuang, Y.-L. Wang, W.-X. Chen, Z.-T. Li, J.-L. Hou, *Nat. Chem.* **2024**, *16*, 1418–1426.
- [41] A. Kohata, K. Kinbara, Nat. Chem. 2024, 16, 1387–1389, https://doi.org/10.1038/s41557-024-01604-y.
- [42] J. Svec, M. Necas, V. Sindelar, Angew. Chem., Int. Ed. 2010, 49, 2378–2381, https://doi.org/10.1002/anie.201000420.
- [43] T. Lizal, V. Sindelar, Isr. J. Chem. 2018, 58, 326–333, https://doi. org/10.1002/ijch.201700111.
- [44] O. Reany, A. Mohite, E. Keinan, Isr. J. Chem. 2018, 58, 449–460, https://doi.org/10.1002/ijch.201700138.
- [45] J. Torrisi, M. Chvojka, P. Jurček, X. Zhang, H. Zeng, V. Šindelář, H. Valkenier, *Angew. Chem., Int. Ed.* 2025, 64, e202424754, https://doi.org/10.1002/anie.202424754.
- [46] M. Singh, E. Solel, E. Keinan, O. Reany, Chem. Eur. J. 2015, 21, 536–540.
- [47] M. Singh, E. Solel, E. Keinan, O. Reany, Chem. Eur. J. 2016, 22, 8848–8854.
- [48] R. Khurana, F. Yang, R. Khurana, J. Liu, E. Keinan, O. Reany, Chem. Commun. 2022, 58, 3150–3153, https://doi.org/10.1039/ D2CC00144F.
- [49] P. V. Jog, M. S. Gin, Org. Lett. 2008, 10, 3693–3696, https://doi. org/10.1021/ol8013045.
- [50] R.-Y. Yang, C.-Y. Bao, Q.-N. Lin, L.-Y. Zhu, Chin. Chem. Lett. 2015, 26, 851–856, https://doi.org/10.1016/j.cclet.2015.05.010.
- [51] J. N. Martins, B. Raimundo, A. Rioboo, Y. Folgar-Cameán, J. Montenegro, N. Basílio, J. Am. Chem. Soc. 2023, 145, 13126–13133, https://doi.org/10.1021/jacs.3c01829.
- [52] L. Husaru, R. Schulze, G. Steiner, T. Wolff, W. D. Habicher, R. Salzer, *Anal. Bioanal. Chem.* 2005, 382, 1882–1888, https://doi.org/10.1007/s00216-005-3380-4.
- [53] C. Lang, A. Mohite, X. Deng, F. Yang, Z. Dong, J. Xu, J. Liu, E. Keinan, O. Reany, *Chem. Commun.* 2017, 53, 7557–7560, https://doi.org/10.1039/C7CC04026A.
- [54] W. Szymański, J. M. Beierle, H. A. V. Kistemaker, W. A. Velema, B. L. Feringa, *Chem. Rev.* 2013, 113, 6114–6178, https://doi.org/ 10.1021/cr300179f.
- [55] H. M. D. Bandara, S. C. Burdette, Chem. Soc. Rev. 2012, 41, 1809–1825, https://doi.org/10.1039/C1CS15179G.

- [56] C. Ren, X. Ding, A. Roy, J. Shen, S. Zhou, F. Chen, S. F. Yau Li, H. Ren, Y. Y. Yang, H. Zeng, *Chem. Sci.* 2018, 9, 4044–4051, https://doi.org/10.1039/C8SC00602D.
- [57] Z. Chen, X. Xie, C. Jia, Q. Zhong, Q. Zhang, D. Luo, Y. Cao, Y. Mu, C. Ren, *Angew. Chem., Int. Ed.* 2024, 63, e202318811, https://doi.org/10.1002/anie.202318811.
- [58] X. Wu, P. A. Gale, J. Am. Chem. Soc. 2016, 138, 16508–16514, https://doi.org/10.1021/jacs.6b10615.
- [59] E. N. W. Howe, P. A. Gale, J. Am. Chem. Soc. 2019, 141, 10654– 10660, https://doi.org/10.1021/jacs.9b02116.
- [60] X. Wu, L. W. Judd, E. N. W. Howe, A. M. Withecombe, V. Soto-Cerrato, H. Li, N. Busschaert, H. Valkenier, R. Pérez-Tomás, D. N. Sheppard, Y.-B. Jiang, A. P. Davis, P. A. Gale, *Chem* 2016, 1, 127–146.
- [61] C. McKenzie, I. Sanchez-Romero, H. Janovjak, Flipping the Photoswitch: Ion Channels Under Light Control in Novel Chemical Tools to Study Ion Channel Biology. Advances in Experimental Medicine and Biology, (Eds:C. Ahern, S. Pless), Vol. 869. Springer, New York 2015.
- [62] C. Engelhard, I. Chizhov, F. Siebert, M. Engelhard, *Chem. Rev.* 2018, 118, 10629–10645, https://doi.org/10.1021/acs.chemrev. 7b00715.
- [63] E. G. Govorunova, O. A. Sineshchekov, R. Janz, X. Liu, J. L. Spudich, *Science* 2015, 349, 647–650, https://doi.org/10.1126/ science.aaa7484.
- [64] S. Oiki, in Patch Clamp Techniques: From Beginning to Advanced Protocols (Ed.: Y. Okada), Springer Japan, Tokyo 2012, pp. 229–275.
- [65] S.-K. Ko, S. K. Kim, A. Share, V. M. Lynch, J. Park, W. Namkung, W. Van Rossom, N. Busschaert, P. A. Gale, J. L. Sessler, I. Shin, *Nat. Chem.* 2014, 6, 885–892, https://doi.org/10.1038/ nchem/2021
- [66] N. Busschaert, S.-H. Park, K.-H. Baek, Y. P. Choi, J. Park, E. N. W. Howe, J. R. Hiscock, L. E. Karagiannidis, I. Marques, V. Félix, W. Namkung, J. L. Sessler, P. A. Gale, I. Shin, *Nat. Chem.* 2017, 9, 667–675, https://doi.org/10.1038/nchem.2706.
- [67] A. Mondal, S. N. Save, S. Sarkar, D. Mondal, J. Mondal, S. Sharma, P. Talukdar, J. Am. Chem. Soc. 2023, 145, 9737–9745, https://doi.org/10.1021/jacs.3c01451.
- [68] Q. Zhong, Y. Cao, X. Xie, Y. Wu, Z. Chen, Q. Zhang, C. Jia, Z. Wu, P. Xin, X. Yan, Z. Zeng, C. Ren, Angew. Chem., Int. Ed. 2024, 63, e202314666, https://doi.org/10.1002/anie.202314666.
- [69] C. Jia, D. Luo, J. Zhou, X. Xie, H. Yuen In Lam, P. Li, Y. Mu, Z. Zeng, C. Ren, Angew. Chem., Int. Ed. 2024, n/a, e202419800.
- [70] W. G. Ryder, A. Levina, M. E. Graziotto, B. A. Hawkins, D. E. Hibbs, E. J. New, P. A. Gale, *Chem* 2024, 102247.
- [71] S. B. Salunke, J. A. Malla, P. Talukdar, Angew. Chem., Int. Ed. 2019, 58, 5354–5358, https://doi.org/10.1002/anie.201900869.
- [72] A. R. Graves, P. K. Curran, C. L. Smith, J. A. Mindell, *Nature* 2008, 453, 788–792, https://doi.org/10.1038/nature06907.
- [73] Y. Ishida, S. Nayak, J. A. Mindell, M. Grabe, J. Gen. Physiol. 2013, 141, 705–720, https://doi.org/10.1085/jgp.201210930.
- [74] S. Hosogi, K. Kusuzaki, T. Inui, X. Wang, Y. Marunaka, J. Cell. Mol. Med. 2014, 18, 1124–1133, https://doi.org/10.1111/jcmm. 12257.
- [75] K.-H. Baek, J. Park, I. Shin, Chem. Soc. Rev. 2012, 41, 3245, https://doi.org/10.1039/c2cs15328a.
- [76] J. Yang, G. Yu, J. L. Sessler, I. Shin, P. A. Gale, F. Huang, *Chem* 2021, 7, 3256–3291, https://doi.org/10.1016/j.chempr.2021.10.028.
- [77] A. Mondal, M. Ahmad, D. Mondal, P. Talukdar, Chem. Commun. 2023, 59, 1917–1938, https://doi.org/10.1039/D2CC06761G.

Manuscript received: August 31, 2025 Revised manuscript received: September 26, 2025 Manuscript accepted: September 30, 2025 Version of record online: